Geophys. J. Int. (1996) **125**, 1–14

Coseismic deformation from earthquake faulting on a layered spherical earth

Fred F. Pollitz

Institute of Theoretical Geophysics, University of Cambridge, Department of Earth Sciences, Downing Street, Cambridge CB2 3EQ, *UK*

Accepted 1995 September 21. Received 1995 September 18; in original form 1995 July 26

SUMMARY

A method for calculating the static displacement field following earthquake faulting in a layered spherical earth is presented. At shallow levels, the Earth's layering is characterized by sharp jumps in bulk and shear moduli at the Conrad discontinuity and the Moho and is therefore important to consider when evaluating crustal deformation. The solution to the equations of static equilibrium is represented as a superposition of spheroidal and toroidal components that each depend on spherical harmonic degree and the moment tensor. A method that has recently been applied to the problem of wave propagation on a layered spherical earth is here applied to the static deformation field. By representing the point source in terms of discontinuities in the displacement–stress vector, the Green's function for a particular source geometry is derived directly. Numerical tests are presented to verify the accuracy of the method and to illustrate the effects of sphericity and layering on the calculated deformation fields. The effect of sphericity is generally less than about 2 per cent (of maximum deformation) within 100 km of an earthquake source at crustal depths. Comparisons between the deformation calculated on a spherical homogeneous earth and spherical layered earth show that up to 20 per cent errors would be introduced if the Earth's layered structure were ignored. The effect of layering is strongest for sources with a strong horizontal slip component.

Key words: deformation, Green's functions, layered media.

INTRODUCTION

The static deformation of the Earth from a buried earthquake source has in recent years received several different formulations for both a homogeneous and a layered half-space. Okada (1985) presented analytic formulae for surface displacements and strains for buried earthquake sources in a homogeneous half-space, and Okada (1992) extended this to observations made at depth. In an isotropic layered half-space, serveral investigators have made use of propagator matrix methods in cylindrical coordinates (Singh 1970; Jovanovich, Husseini & Chinnery 1974a, b; Singh & Garg 1985; Rundle 1980) to obtain analytic solutions for the static displacements and strains. Rundle's treatment includes a zeroth-order coupling between the elastic and gravitational forces. Similarly, Matsu'ura, Tanimoto & Iwasaki (1981) specified an analytic method for calculating the displacement field in a layered half-space for general earthquake sources (that is, for the six independent elements of the moment tensor in an isotropic medium). A more general formulation in Cartesian coordinates for a transversely isotropic medium was presented by Pan (1989). Reviews of progress in applying elastic dislocation theory to the static response of a homogeneous or layered half-space may be found in Okada (1985) and Pan (1989). Since geodetic observations modelled with such calculations have been, in the majority of cases, close to the faulting sources, a homogeneous half-space has been justified in most studies, and the formulations of Okada have received widespread application.

Geodetic observations made at moderate distances from a fault could benefit from a modelling procedure which accounts for the layering in elastic parameters in the Earth, particularly the sharp increases in bulk and shear moduli at the Conrad discontinuity and the Moho. Yoshioka, Hashimoto & Hirahara (1989) recently made this point effectively for modelling of horizontal deformation in southwest Japan. Recent space-based geodetic techniques have greatly extended the spatial range and density of measurements that are sensitive to fault movements. The objective of this paper is to present a method of calculating the static displacement field on a layered spherical earth from a buried earthquake source, given a general moment tensor. The solution of this problem and additional motivation have been detailed previously by Wason & Singh (1972). Here I give a more compact presentation of the various

steps involved in the solution, together with several examples. The use of a spherical earth geometry considerably simplifies the number of steps involved with the calculation of the static deformation fields. In particular, we may express the solution conveniently as a sum of spherical harmonic components, and it is relatively straightforward to express the appropriate boundary conditions for each component. The relative simplicity of the described method could make it applicable to problems in crustal deformation on a more systematic basis than the half-space formulations. Although the effect of the Earth's sphericity is found to be slight for near-field crustal deformation, the new treatment could find application in modelling the deformation following very deep earthquakes, such as the 1994 Bolivian earthquake. Except for an application to a layered elastic plate, coupling between gravitation and elasticity is ignored here. This is an excellent approximation for most conceivable applications involving unrelaxed deformation. Any extension of the method presented here to the problem of viscoelastic relaxation would benefit from the inclusion of the effects of gravity (Rundle 1980, 1982).

In the following sections, I shall give the details of the computational method, followed by numerical tests. Comparisons with the exact solution for a homogeneous half-space will demonstrate the accuracy of the method, and comparisons between the deformation calculated on the layered and homogeneous earth models will illuminate the errors involved with ignoring the Earth's layered structure.

THEORY

We work throughout in a spherical earth geometry in an epicentral coordinate system (Fig. 1). Let r denote the radius and θ and ϕ the colatitude and longitude, respectively, of an observation point $\mathbf{r}=(r,\theta,\phi)$ relative to a specified point source. The source at $\mathbf{r}_s$ has coordinates $(r=r_s,\theta=0)$. It is assumed that bulk modulus $\kappa(r)$ and shear modulus $\mu(r)$ are laterally homogeneous, depending only on radius.

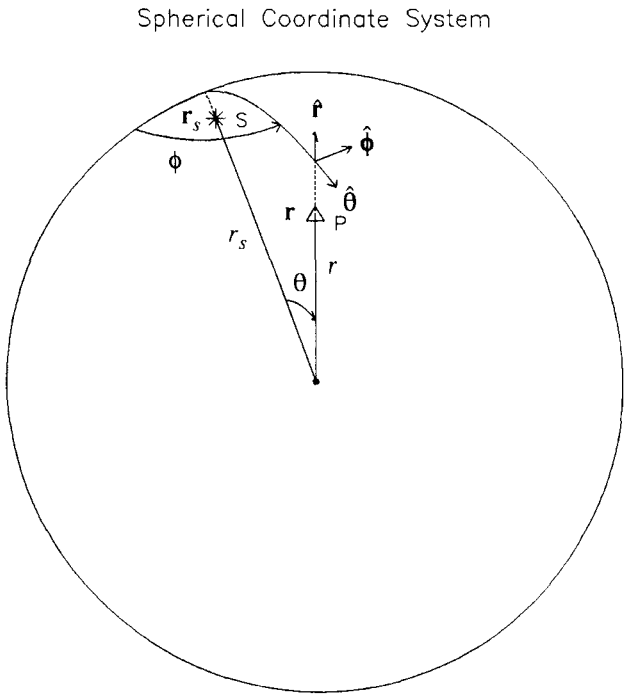

Figure 1. Spherical coordinate and source geometry. The Earth's radius a is taken to be 6371 km.

The displacement field for a point dislocation is obtained as a summation of normal modes. Let $Y_l^m(\theta,\phi)$ represent the fully normalized spherical harmonic of total degree l and azimuthal order number m (Edmonds 1960). Explicitly, for positive m we define

$$Y_l^m(\theta,\phi)=(-1)^m\left[\frac{2l+1}{4\pi}\frac{(l-m)!}{(l+m)!}\right]^{1/2}P_l^m(\cos\theta)\,e^{im\phi}, \tag{1}$$

where P_l^m is the associated Legendre polynomial, and

$$Y_l^{-m}(\theta,\phi)=(-1)^m\,Y_l^{m*}(\theta,\phi), \tag{2}$$

where * denotes complex conjugation. Then the displacement field may be represented in terms of a basis set of spheroidal and toroidal modes, with

$$\mathbf{s}_l^{m(\mathrm{S})}(r,\theta,\phi)=[\,y_1^{lm(\mathrm{S})}(r)\hat{\mathbf{r}}+y_3^{lm(\mathrm{S})}(r)\nabla_1\,]\,Y_l^m(\theta,\phi) \tag{3a}$$

for spheroidal modes, and

$$\mathbf{s}_l^{m(\mathrm{T})}(r,\theta,\phi)=-y_1^{lm(\mathrm{T})}(r)\hat{\mathbf{r}}\times\nabla_1\,Y_l^m(\theta,\phi) \tag{3b}$$

for toroidal modes. In eqs (3), ∇_1 is the surface gradient operator,

$$\nabla_1=\frac{\partial}{\partial\theta}\hat{\theta}+(\sin\theta)^{-1}\frac{\partial}{\partial\phi}\hat{\phi}. \tag{4}$$

The corresponding normal and shear tractions on the spherical shell of radius r may be expressed in the form

$$\hat{\mathbf{r}}\cdot\boldsymbol{T}_l^{m(\mathrm{S})}(r,\theta,\phi)=[\,y_2^{lm(\mathrm{S})}(r)\hat{\mathbf{r}}+y_4^{lm(\mathrm{S})}(r)\nabla_1\,]\,Y_l^m(\theta,\phi) \tag{5a}$$

for spheroidal modes, and

$$\hat{\mathbf{r}}\cdot\boldsymbol{T}_l^{m(\mathrm{T})}(r,\theta,\phi)=-y_2^{lm(\mathrm{T})}(r)\hat{\mathbf{r}}\times\nabla_1\,Y_l^m(\theta,\phi) \tag{5b}$$

for toroidal modes, where $\boldsymbol{T}$ denotes the stress tensor in an isotropic medium. The total displacement field is given by

$$\mathbf{s}(r,\theta,\phi)=\sum_l\sum_m\mathbf{s}_l^{m(\mathrm{S})}(r,\theta,\phi)+\mathbf{s}_l^{m(\mathrm{T})}(r,\theta,\phi). \tag{6}$$

In the subsequent development, l and m are taken to be fixed unless indicated otherwise. Also, with the mode type under discussion understood, the superscripts (S) and (T) will be dropped.

The equation of static equilibrium has the form

$$\nabla\cdot\boldsymbol{T}(\mathbf{r})=\boldsymbol{M}\cdot\nabla\delta(\mathbf{r}-\mathbf{r}_s), \tag{7}$$

where $\boldsymbol{M}$ is the moment tensor. This is subject to the boundary conditions $\hat{\mathbf{r}}\cdot\boldsymbol{T}(a)=0$ (where a is the Earth's radius) and the solution must be regular at the origin $r=0$. Defining the displacement–stress vector via

$$\mathbf{y}(r)=[\,y_1(r),\,y_2(r),\,y_3(r),\,y_4(r)\,]^{\mathrm{T}} \tag{8}$$

for spheroidal modes, and

$$\mathbf{y}(r)=[\,y_1(r),\,y_2(r)\,]^{\mathrm{T}} \tag{9}$$

for toroidal modes, (7) may be rewritten as a system of six first-order ordinary differential equations (SODE), with a source term $\mathbf{f}$ at $r=r_s$,

$$\frac{d\mathbf{y}(r)}{dr}=\mathbf{A}(r)\mathbf{y}(r)+\mathbf{f}, \tag{10}$$

where $\mathbf{A}$ is a 4×4 matrix for spheroidal modes and 2×2

matrix for toroidal modes. These are given by the upper 4×4 matrix of eq. (43) of Pollitz (1992) or eq. (35) of that paper (note that a factor r^{-2} must be included in the A_{21} component printed in that equation), both of which correspond to the static case. Derivations of these matrix elements have been given by Takeuchi & Saito (1972) and Lapwood & Usami (1981). The explicit form of the source term has been derived by Friederich & Dalkolmo (1995), who also describe the method of solution of (7) for the case of wave propagation (in which case **A** in eq. 10 has terms which depend on frequency). Except at the source radius, eq. (10) is a homogeneous SODE. In the static case, where the frequency dependence of **A** vanishes, the solution of this homogeneous SODE is given by the layer matrix solutions of Pollitz (1992, eqs 36–40 and 49–52).

For spheroidal modes, there exist two linearly independent solutions of (10) for $r < r_s$ and four linearly independent solutions for $r > r_s$. There are two boundary conditions at the surface,

$$y_2(a) = y_4(a) = 0, \tag{11}$$

and four boundary conditions at the source, which together determine the unknown coefficients which weigh the six independent solutions.

For toroidal modes, there exists one solution of (8) for $r < r_s$ and two linearly independent solutions for $r > r_s$. There is one boundary condition at the surface,

$$y_2(a) = 0, \tag{12}$$

and two boundary conditions at the source.

The source boundary conditions specify the jump in displacement–stress vector across the source radius

$$\Delta\mathbf{y} = \mathbf{y}(r_s^+) - \mathbf{y}(r_s^-), \tag{13}$$

where r_s^+ and r_s^- denote evaluation just above or below the source radius. The jumps $\Delta\mathbf{y}$ have been specified for a shear dislocation by Ben-Menahem & Singh (1981, p. 217). This solution completely specifies the required source boundary conditions for the toroidal modes, which are not sensitive to isotropic source components. To completely specify the jumps for spheroidal modes, we must append these solutions with one which corresponds to a moment tensor with an isotropic component. The simplest is to consider a source composed of three dipoles, such that horizontal strain at the source is zero and only vertical strain e_{rr} is non-zero.
That is,

$$e_{\theta\theta} = e_{\phi\phi} = e_{\theta\phi} = e_{r\theta} = e_{r\phi} = 0,$$
$$e_{rr} \text{ non-zero}. \tag{14}$$

The strain component e_{rr} may be written in terms of the stress tensor via

$$e_{rr}(\mathbf{r}) = \frac{1}{3\kappa\mu}\left[(\lambda+\mu)T_{rr}(\mathbf{r}) - \frac{\lambda}{2}[T_{\theta\theta}(\mathbf{r}) + T_{\phi\phi}(\mathbf{r})]\right], \tag{15}$$

where $\lambda = \kappa - \frac{2}{3}\mu$, and in terms of $\mathbf{y}$ via

$$e_{rr}(\mathbf{r}) = \sum_l \sum_m \partial_r y_1^{lm(S)}(r) Y_l^m(\theta, \phi), \tag{16}$$

where ∂_r denotes partial differentiation with respect to r. By multiplying eqs (7) and (15) by $Y_l^{m*}(\theta, \phi)$, integrating them over the volume between two spherical shells of radius $r_s - \delta r$ and $r_s + \delta r (\delta r > 0)$, and taking the limit $\delta r \to 0$, we obtain non-zero $\Delta\mathbf{y}$ only for the components $m = 0$, given by

$$\Delta\mathbf{y} = \begin{bmatrix} \frac{X_l^0(0)}{r_s^2}\frac{1}{3\mu\kappa}\left[(\lambda+\mu)M_{rr} - \frac{\lambda}{2}(M_{\theta\theta}+M_{\phi\phi})\right] \\ 0 \\ 0 \\ 0 \end{bmatrix}. \tag{17}$$

The X_l^m that appear in (17) and below are related to the spherical harmonics via $Y_l^m(\theta, \phi) = X_l^m(\theta)\exp(im\phi)$, where the Y_l^m are defined by eq. (1). This solution, plus that for a shear dislocation, are sufficient to specify $\Delta\mathbf{y}$ for spheroidal modes and toroidal modes for a general moment tensor. These are non-zero only for $m = 0$, ± 1, or ± 2, and are specified for non-negative m as follows.

Spheroidal modes:

***m* = 0**

$$\Delta\mathbf{y} = \begin{bmatrix} \frac{X_l^0(0)}{r_s^2}\frac{1}{\lambda+2\mu}M_{rr} \\ \frac{X_l^0(0)}{r_s^2}\left(\frac{-2\mu}{r_s}\right)\left(3 - \frac{4\mu}{\lambda+2\mu}\right)\frac{1}{3\mu\kappa} \\ \quad \times\left[-\lambda M_{rr} + \left(\frac{\lambda}{2}+\mu\right)(M_{\theta\theta}+M_{\phi\phi})\right] \\ 0 \\ \frac{X_l^0(0)}{r_s^2}\left(\frac{\mu}{r_s}\right)\left(3 - \frac{4\mu}{\lambda+2\mu}\right)\frac{1}{3\mu\kappa} \\ \quad \times\left[-\lambda M_{rr} + \left(\frac{\lambda}{2}+\mu\right)(M_{\theta\theta}+M_{\phi\phi})\right] \end{bmatrix}, \tag{18}$$

***m* = 1**

$$\Delta\mathbf{y} = \begin{bmatrix} 0 \\ 0 \\ \frac{\partial_\theta X_l^1(0)}{r_s^2}\frac{1}{\mu l(l+1)}[M_{r\theta} - iM_{r\phi}] \\ 0 \end{bmatrix}, \tag{19}$$

***m* = 2**

$$\Delta\mathbf{y} = \begin{bmatrix} 0 \\ 0 \\ 0 \\ -\frac{\partial_{\theta\theta} X_l^2(0)}{r_s^3}\frac{1}{l(l+1)}[M_{\theta\theta} - M_{\phi\phi} - 2iM_{\theta\phi}] \end{bmatrix}. \tag{20}$$

Toroidal modes:

***m* = 1**

$$\Delta\mathbf{y} = \begin{bmatrix} \frac{\partial_\theta X_l^1(0)}{r_s^2}\frac{1}{\mu l(l+1)}[-M_{r\phi} - iM_{r\theta}] \\ 0 \end{bmatrix}, \tag{21}$$

$\boldsymbol{m=2}$

$$\Delta\mathbf{y}=\begin{bmatrix} 0 \\ \dfrac{\partial_{\theta\theta}X_l^2(0)}{r_s^3}\dfrac{1}{l(l+1)}i[M_{\theta\theta}-M_{\phi\phi}-2iM_{\theta\phi}] \end{bmatrix}. \tag{22}$$

The quantities X_l^0, $\partial_\theta X_l^1$, and $\partial_{\theta\theta}X_l^2$ have the values

$$\lim_{\theta\to 0} X_l^0(\theta)=\left[\frac{2l+1}{4\pi}\right]^{1/2},$$

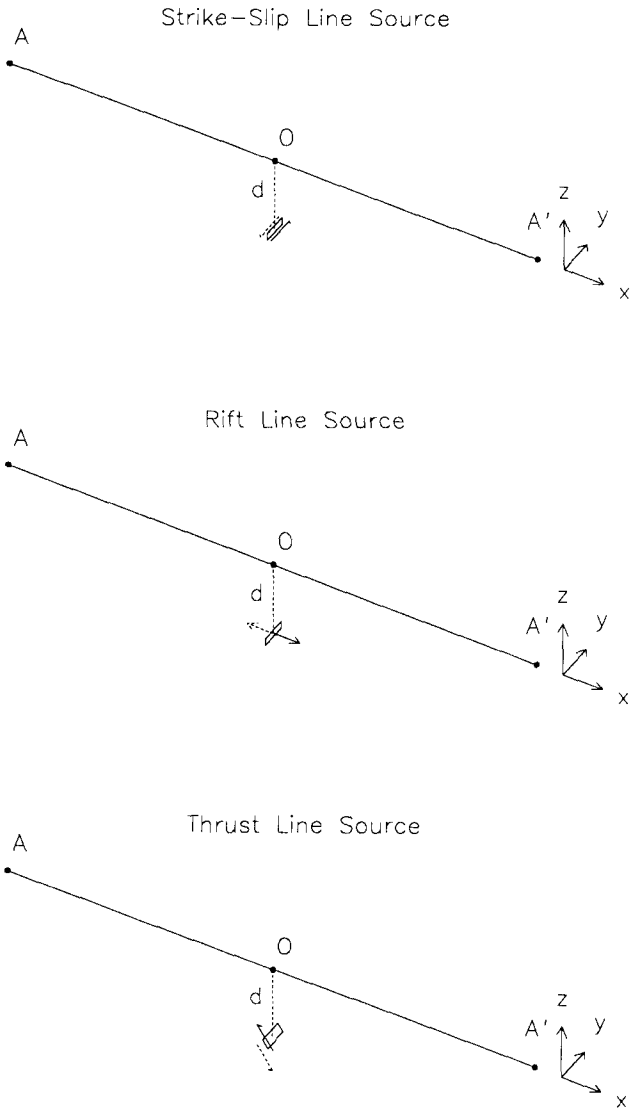

Figure 2. Three candidate source geometries used in the examples. Each line source extends from $y=-5$ to $y=5$ and is buried a depth d below the surface. The width of each fault is taken as infinitesimally small, such that the product of the width and slip is a constant. The dip of the strike-slip and rift faults is 90°, and the dip of the thrust fault is 45°. The seismic moment for sources shallower than 16 km has the values 1.02×10^{17} N m (thrust), 0.720×10^{17} N m (strike-slip), and 1.80×10^{17} N m (rift). Profile AA' is taken on the planar or spherical surface of the earth parallel to the x axis and passing through the origin O, which is the source epicentre. For calculations on the spherical earth, O is taken on the equator in a geographic coordinate system, and the x, y and z axes are locally parallel to the due East, due North, and upward directions, respectively.

$$\lim_{\theta\to 0}\partial_\theta X_l^1(\theta)=\frac{-1}{2}\left[\frac{2l+1}{4\pi}\right]^{1/2}[l(l+1)]^{1/2}, \tag{23}$$

$$\lim_{\theta\to 0}\partial_{\theta\theta}X_l^2(\theta)=\frac{1}{4}\left[\frac{2l+1}{4\pi}\right]^{1/2}[l(l-1)(l+1)(l+2)]^{1/2}.$$

The m summation for displacements and stresses in eqs (3a)–(3b) and (5a)–(5b) is from -2 to 2, and the jumps for negative m are formally obtained from eqs (18)–(22) and

$$\Delta\mathbf{y}^{l(-m)}=(-1)^m(\Delta\mathbf{y}^{lm})^*. \tag{24}$$

Note that when the moment tensor is specified in geographic coordinates, as we have assumed, then the longitude ϕ in eqs (3) and (5) represents the source–receiver azimuth measured counterclockwise from due South.

The equivalence of (18)–(22) to the source jumps given by Ben-Menahem & Singh (1981, p. 217) for a shear dislocation may be obtained by transforming their summation convention (which goes from 0 to 2), spherical harmonic and scale parameter conventions to our summation convention (which goes from -2 to 2) and spherical harmonic conventions (eqs 1 and 2). For example, their equations (4.179) and (4.181) for

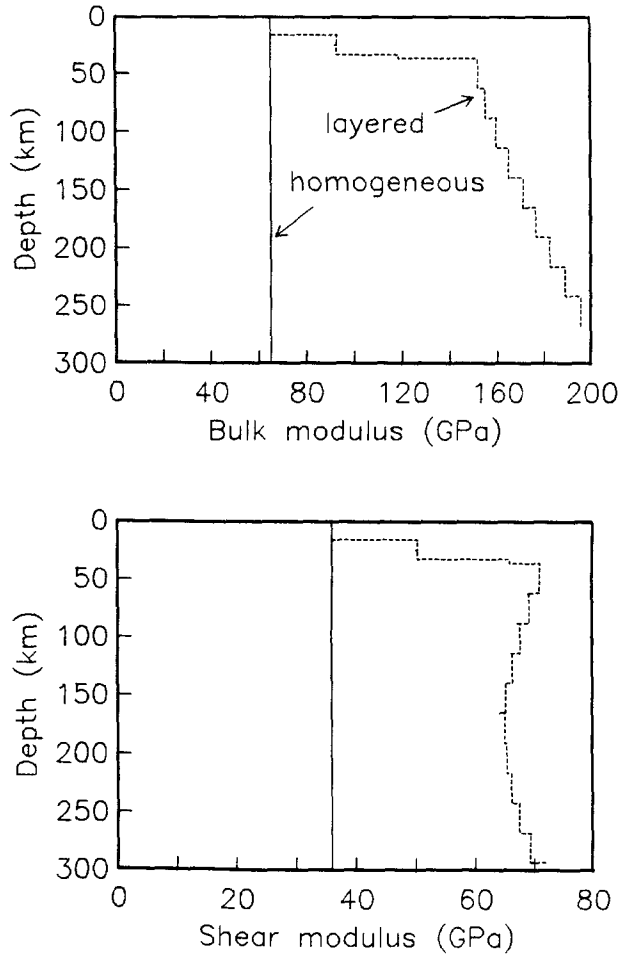

Figure 3. Distribution of isotropic elastic parameters with depth, shown for the upper 300 km of the Earth. The earth model used is a discretized version of the mantle portion of Model 1066A (Gilbert & Dziewonski 1975), with modifications for a continental crust. The solid lines give the constant values of 36 GPa and 65 GPa for shear and bulk modulus, respectively, on the homogeneous earth models.

the source jumps for spheroidal modes from pure dip-slip on a vertical fault may be converted to our conventions by inserting (in their notation) rake $\lambda = -\pi/2$ and dip $\delta = \pi/2$ into these formulae, leading to $\Delta y_1 = \Delta y_2 = \Delta y_4 = 0$ and

$$\Delta y_3 = \frac{1}{2}(2l+1)\Omega_{1l} b^{s}_{1l}(-i)\left[\frac{u_0\, dS}{4\pi r_0^2}\right].$$

The factor 1/2 arises from the difference in summation convention, and the factor $(-i)$ corresponds to their 'sine' solution in longitude ϕ. Taking a north–south striking fault, we have

$$\Omega_{1l} = \sqrt{\frac{4\pi}{2l+1}\, l(l+1)},$$

$$b^{s}_{1l} = \frac{1}{l(l+1)},$$

$$\frac{u_0\, dS}{4\pi r_0^2} = \frac{M_{r\phi}}{4\pi r_s^2 \mu},$$

yielding the $M_{r\phi}$ term of eq. (19). Taking an east–west striking fault yields the $M_{r\theta}$ term of (19).

As an additional check on the spheroidal mode jumps for sources with an isotropic component, the values of displacement jump Δy_1 and shear stress jump Δy_4 for a purely isotropic source can be derived independently and compared with (18). Putting an isotropic source at $\mathbf{r} = \mathbf{r}_s$ with non-zero moment tensor elements $M_{rr} = M_{\theta\theta} = M_{\phi\phi} = M$, the displacement field takes the form (Aki & Richards 1980, eq. 4.29)

$$\mathbf{s}(\mathbf{r}) = \frac{M(\mathbf{r} - \mathbf{r}_s)}{4\pi(\lambda + 2\mu)|\mathbf{r} - \mathbf{r}_s|^3}. \tag{25}$$

The jumps are non-zero only for the spheroidal $(l, m = 0)$ components and may be obtained directly by evaluating the limits

$$\begin{aligned} &\iint \hat{\mathbf{r}} \cdot [\mathbf{s}(\mathbf{r}^+) - \mathbf{s}(\mathbf{r}^-)] X^0_l(\theta)\, dA, \\ &\iint \hat{\mathbf{r}} \cdot [\mathbf{T}(\mathbf{r}^+) - \mathbf{T}(\mathbf{r}^-)] \cdot \hat{\theta}\partial_\theta X^0_l(\theta)\, dA, \end{aligned} \tag{26}$$

where $\mathbf{r}^+/\mathbf{r}^-$ denotes evaluation just above/below the spherical shell at radius r_s, over which the integration is carried out.

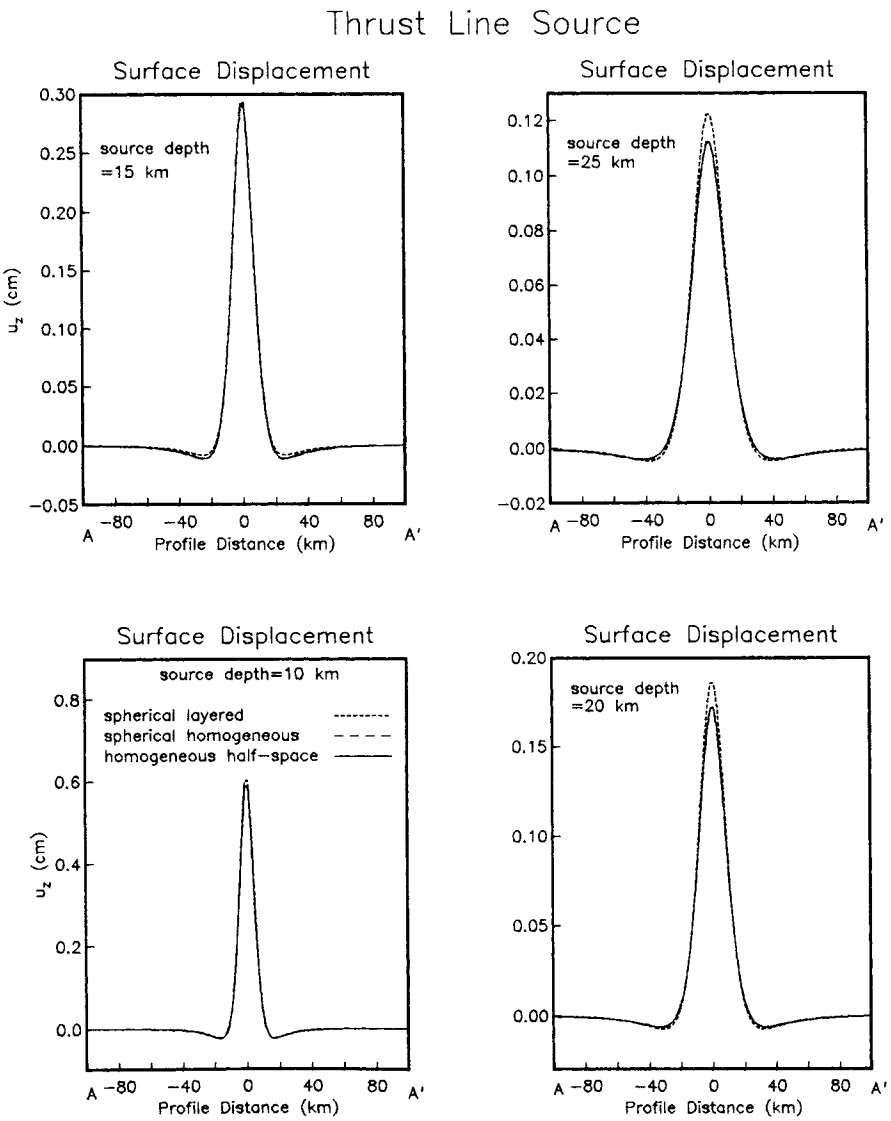

Figure 4. Vertical displacement u_z along profile AA' for a thrust line source buried at different depths.

Applying the integrations in (26) to the displacement fields in the form (3a) and (25) yields

$$\Delta y_1 = \frac{1}{r_s^2} X_l^0(0) \frac{M}{\lambda + 2\mu},$$
$$\Delta y_4 = \frac{2}{r_s^3} X_l^0(0) \frac{M\mu}{\lambda + 2\mu}. \quad (27)$$

These jumps agree with eq. (18). The jump Δy_2 is not directly obtainable using a limit of the form (26) because the integrals in that case are unbounded on both sides as the spherical shell $r = r_s$ is approached.

Finally, the source jumps (18)–(20) agree with those derived by Dalkolmo (1993, his eqs 3.9–3.11) for spheroidal modes, when care is taken to note the slightly different conventions for the spherical harmonics.

NUMERICAL TESTS

In the following tests we shall calculate displacements and strains for some simple fault geometries using our approach on the spherical earth. The surface deformation on both spherical homogeneous and spherical layered earth models will be compared with that on a homogeneous half-space, calculated using the formulae of Okada (1985). These tests will enable us to evaluate the effects of sphericity and layering on predicted deformation.

From a practical viewpoint, the integration of the homogeneous SODE need not extend more than a few wavelengths from the source radius, particularly for the deepest spherical shell where the integration of the $r < r_s$ solutions is begun. One wavelength is defined here as $2\pi a/(l + 1/2)$, where l is the total degree number. It is found that 2.5 wavelengths is sufficient to estimate the deformation fields with high accuracy. This implies that, for surface observations, if the source is more than 2.5 wavelengths deep, then components of degree l will not contribute to the deformation field. Therefore, for surface observations, the source depth acts as a spatial filter and defines the cut-off degree l (or cut-off wavelength). Similarly, for observations at depth, the integration of the homogeneous SODE is started 2.5 wavelengths beneath the source and propagated up to either the true free surface or a radius 2.5 wavelengths shallower than the source, whichever is deeper. Thus, in general, if the observation depth is not within 2.5 wavelengths of the source then that wavelength will not contribute to the deformation observed there. When the observation depth is sufficiently close to the source depth and the source is buried by more than 2.5 wavelengths beneath the surface, then free-surface boundary conditions are imposed on the spherical shell 2.5 wavelengths above the source radius. A test of this procedure for surface observations is given below and is found to yield very stable results at all observation depths. A similar procedure is outlined by Friederich & Dalkolmo (1995) for the case of wave propagation, in which only low-l PKIKP-equivalent modes are allowed to propagate through the core in their integration of the homogenous SODE.

Three different fault geometries are shown in Fig. 2. In calculations on a spherical earth, the coordinates x and y are taken due East and North, respectively, and the coordinate z the upward normal to the spherical surface. Unless otherwise indicated, the spherical harmonic expansion is truncated at $l = 10\,000$, corresponding to a minimum wavelength of 4 km. The upper 300 km of the earth models used are shown in Fig. 3. On both the spherical homogeneous earth and the

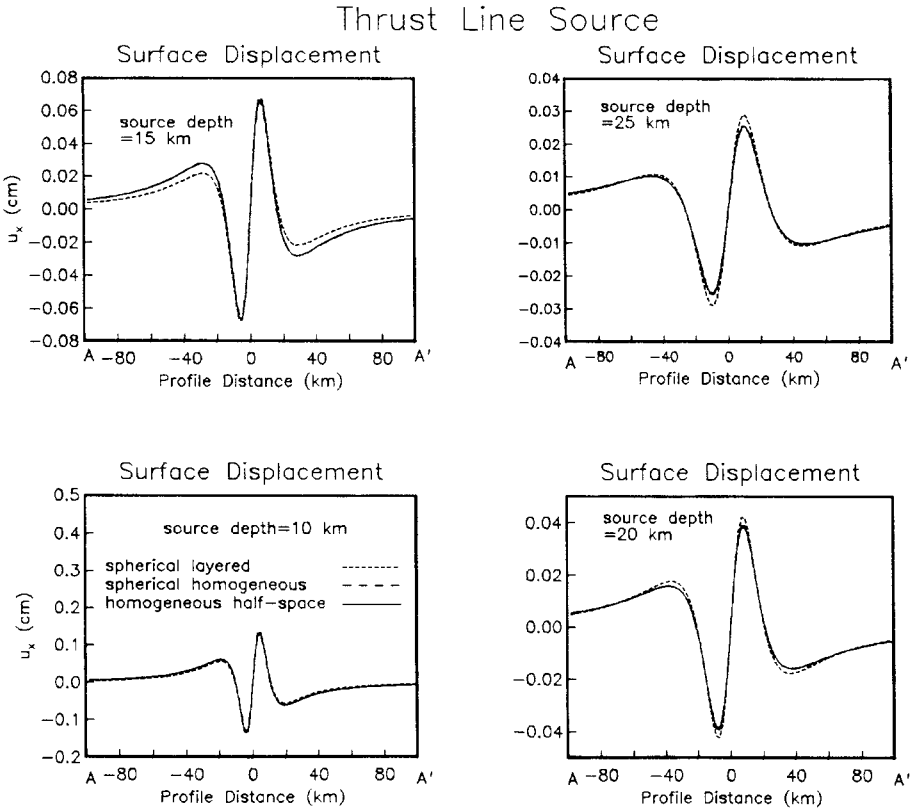

Figure 5. Same as Fig. 4, but for horizontal displacement u_x.

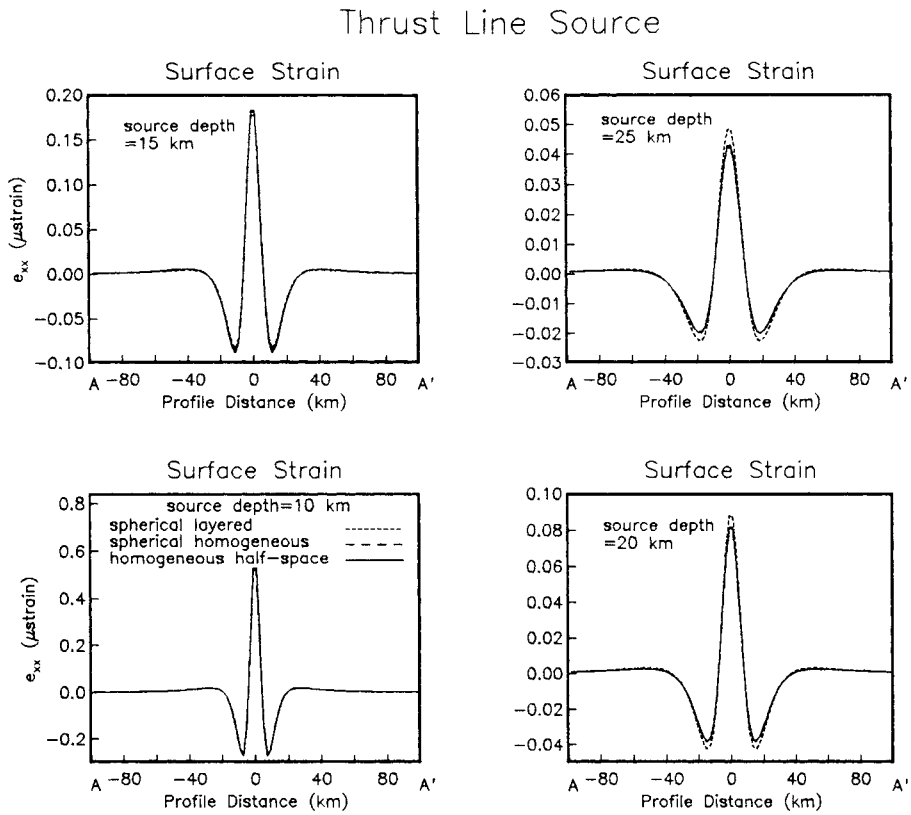

Figure 6. Same as Fig. 4, but for horizontal strain e_{xx}.

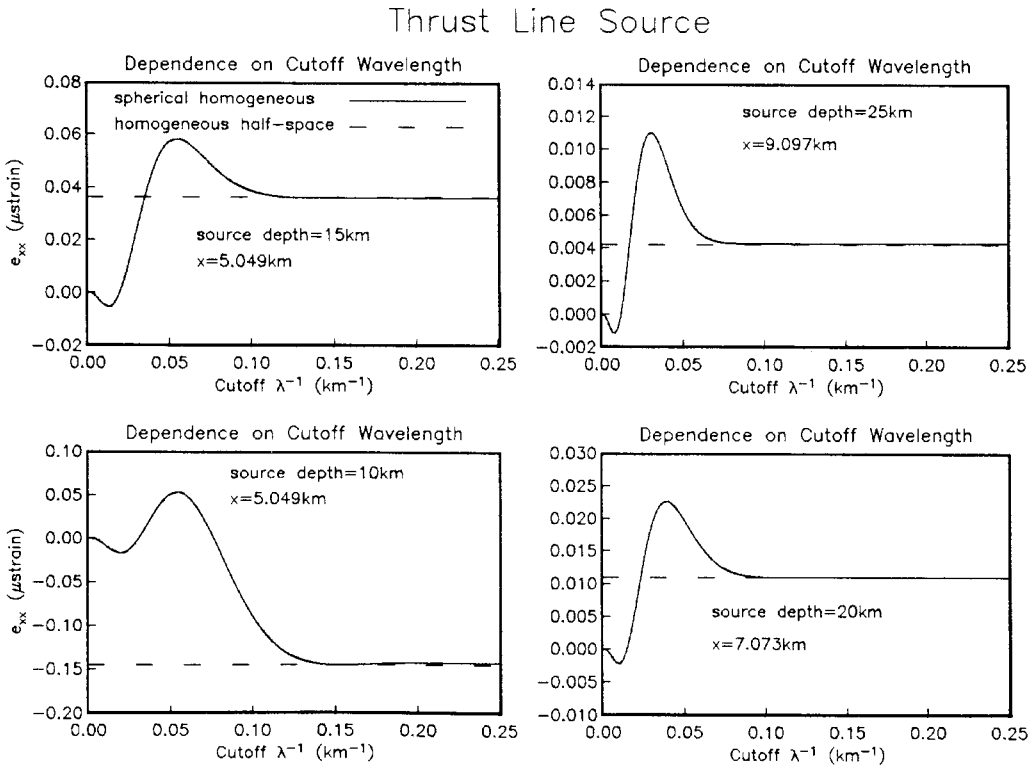

Figure 7. Dependence of e_{xx} on cut-off wavelength λ^{-1}. If l_{max} is the truncation degree in the spherical harmonic expansion (eq. 6), then λ is defined as $2\pi a/(l_{max}+1/2)$. The strain is evaluated for the thrust line source along points on the profile AA' specified by the x coordinate.

homogeneous half-space, constant elastic parameters are assigned; these coincide with the elastic parameters in the layered model in the upper crust (shallower than 16 km). The layered earth model is actually the mantle portion of Model 1066A (Gilbert & Dziewonski 1975), except for small revisions above the Moho (shallower than 33 km depth); below 33 km depth note that the smooth Model 1066A has been approximated by several discrete layers. The line sources each extend from $y = -5$ to $y = 5$ ($x = 0$) at a specified depth d (Fig. 2). In effect, the fault width is taken as infinitesimally small, such that the product of the fault width and slip is a constant. This procedure is preferable to fixing the total moment because moment is proportional to rigidity, in which case slip distributions would be a discontinuous function of fault depth. The seismic moment for sources shallower than 16 km has the values 1.02×10^{17} N m (thrust), 0.720×10^{17} N m (strike-slip), and 1.80×10^{17} N m (rift).

A line source is realized by numerical integration of the appropriate Green's functions for deformation from a point source, given by Okada's (1985) eqs (8)–(16) or our eq. (6). A very fine integration step was used and tested to ensure uniform sampling of the line source.

Results for a thrust line source are shown in Figs 4–6. These results demonstrate that the effect of sphericity for this source type is very small in both horizontal and vertical displacement and horizontal strain e_{xx} out to at least 100 km from the fault, regardless of fault depth. The effect of layering is to slightly reduce displacements and strains for sources shallower than 16 km depth, and to slightly amplify the deformation for sources deeper than 16 km depth. This must reflect the effect of the sharp increase in bulk and shear moduli at 16 km depth. Approximately 10 per cent errors in displacements and strains (relative to the maximum value of deformation) would be introduced by ignoring the Earth's layering.

The effect of truncation of the spherical harmonic expansion was tested by varying the cut-off wavelength. Fig. 7 shows the calculated strain e_{xx} as a function of cut-off wavelength for various source depths. It is clear that the minimum spatial wavelength content of the strain field is roughly proportional to the source depth. The plotted curves were found to be absolutely flat beyond a wavelength of 4 km. I also explored the geographical pattern of the effect of sphericity. This was done by calculating the difference between the spherical homogeneous and homogeneous half-space strain e_{xx} over a 200 km × 200 km grid. The results for several different source depths are shown in Fig. 8. For reference, the profile AA' from Fig. 3 is repeated in the bottom left panel. Since the strain values themselves are of the order of 10^{-2} to 10^{-1}, these results show that the effect of sphericity is generally small for a 45° thrust source at crustal depths out to at least 100 km from the

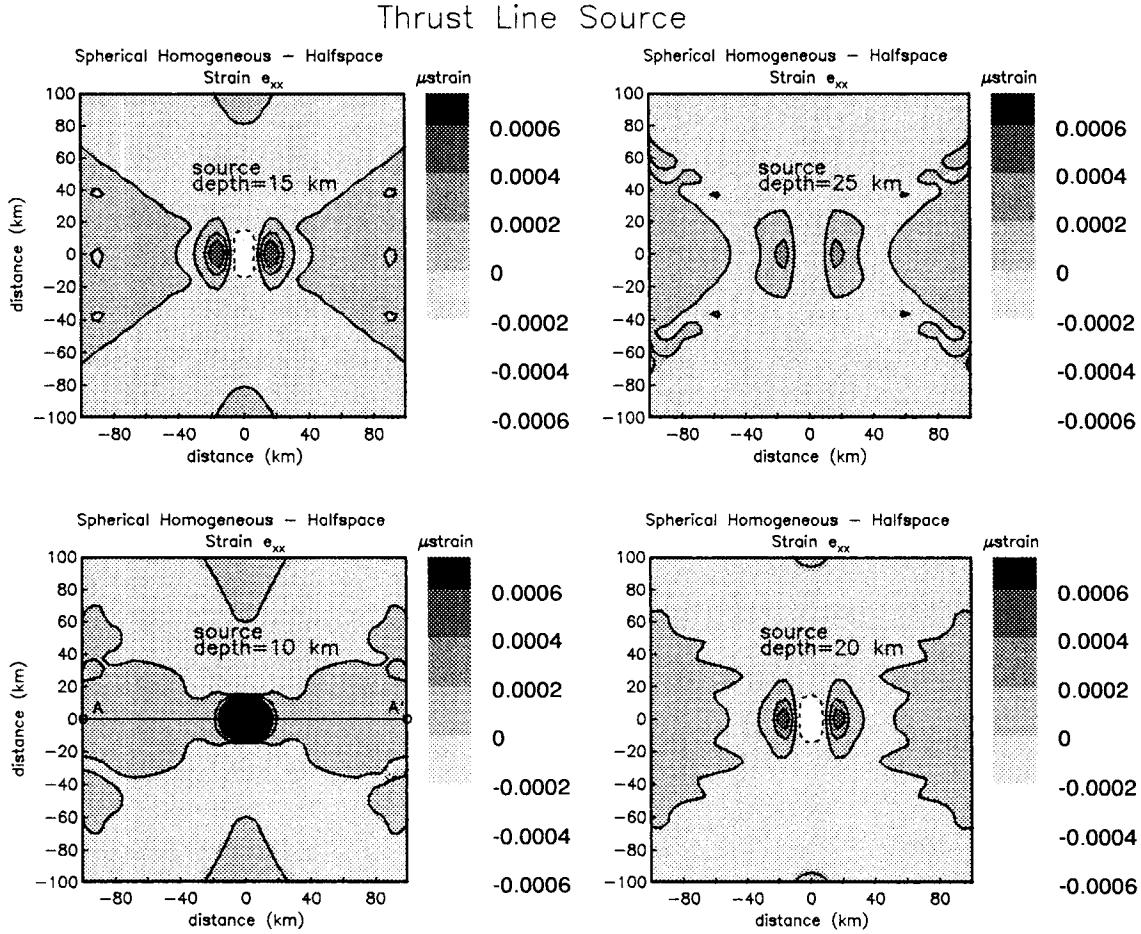

Figure 8. Difference between the strain e_{xx} calculated on the homogeneous sphere and that calculated on the homogeneous half-space, at different source depths. Since the strain values themselves are of the order of 10^{-1} or 10^{-2} (Fig. 6), this shows that the effect of sphericity is quite small out to 100 km from the source.

fault. The ragged spatial patterns far from the fault are very small-amplitude fluctuations and exhibit a wavelength comparable with the cut-off wavelength used in the calculation. The differences between the spherical layered and spherical homogeneous patterns are shown in Fig. 9. This reveals that the geographical distribution of the effect of layering is most pronounced within about 30 km of the fault. Beyond that distance the strains are generally amplified for sources deeper than 16 km, as observed before.

The results of similar calculations for a rift and strike-slip line source are shown in Figs 10 and 11, respectively. The effect of layering is even more pronounced for these two cases. For a source at 20 km depth, the effect of layering is to increase the displacements by 15–20 per cent. As with the other source types, the effect of layering is to reduce the amplitude of the deformation for sources shallower than 16 km, and to increase the amplitude for sources deeper than 16 km.

This amplification/deamplification effect of the layering can be explained in terms of stress localization at the layer boundaries so that, in general, the deformation field within an entire layer exhibits the same response to the interactions above or below the layer. In order to show this, I calculated the deformation from the strike-slip line source on a 40 km × 16 km grid in the xz plane (in the plane $y = 0$) in the upper 16 km of the Earth; that is, shallower than the shallowest layer boundary at $z = -16$ km, taking a source depth of 15.9 km. A cut-off wavelength of 1 km was used. Fig. 12 shows the pattern of y-displacement u_y for both the spherical homogeneous and spherical layered cases, as well as the homogeneous half-space (calculated using the formulae of Okada 1992). Fig. 13 shows the corresponding pattern of shear stress T_{yz}. These patterns are truncated at depth 15.9 km in order to avoid a sharp change in the pattern just below the source radius. In calculating these patterns for a fixed source depth, the radial displacement functions [$y_1(r)$, etc.] were calculated discretely at 1 km depth knots from 0.5 km down to 16.5 km. Cubic spline interpolation was performed for depths falling within this depth range. Because of the jump in shear stress T_{yz} at the source radius, a small distortion is thus expected in the shear stress profiles near 15.9 km depth (Fig. 13). A slight distortion near 15.9 km depth is also expected in the displacement profiles because of the 1 km cut-off wavelength. This is clearly seen as a slight curvature in the displacement profile in the lowermost 1 km in the spherical homogeneous case, as is seen by comparison with the homogeneous half-space (Fig. 12). This was verified by repeating the displacement profiles with a 4 km cut-off wavelength, when it was found that the distortion due to wavelength truncation persisted up to about 11 km depth. Regardless of these small effects, Fig. 12 shows that, in the layered case, displacement is relatively diminished in the entire upper 16 km. Fig. 13 shows that shear stress has a more complicated spatial dependence but is also diminished in the

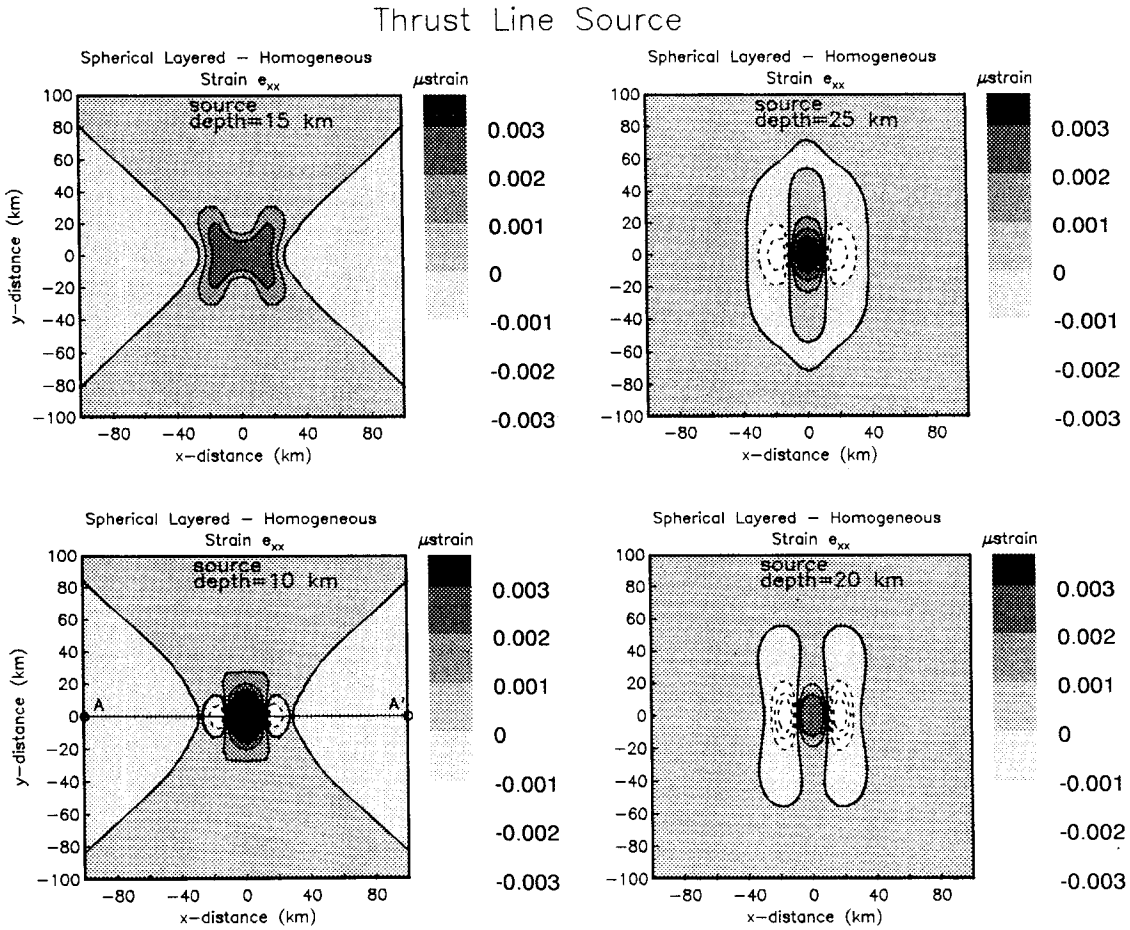

Figure 9. Difference between the strain e_{xx} calculated on the layered sphere and that calculated on the homogeneous sphere, at different source depths.

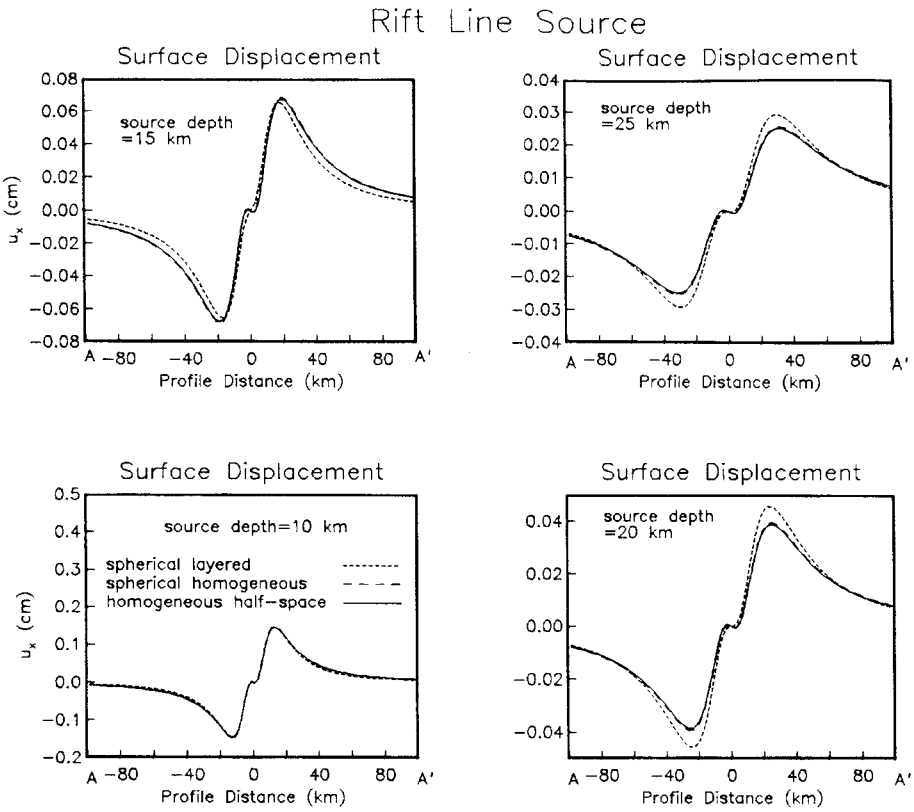

Figure 10. Horizontal displacement u_x along profile AA' for a rift line source buried at different depths.

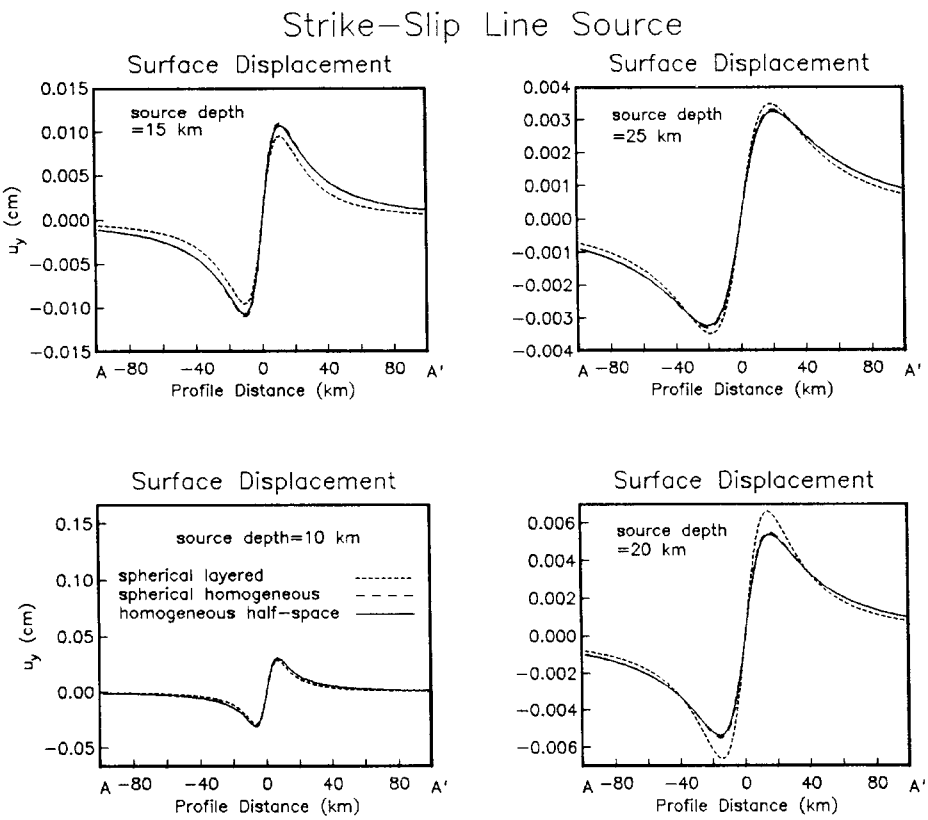

Figure 11. Horizontal displacement u_y along profile AA' for a strike-slip line source buried at different depths. The effect of ignoring the layered structure of the Earth reaches up to 20 per cent of the maximum displacement in this case.

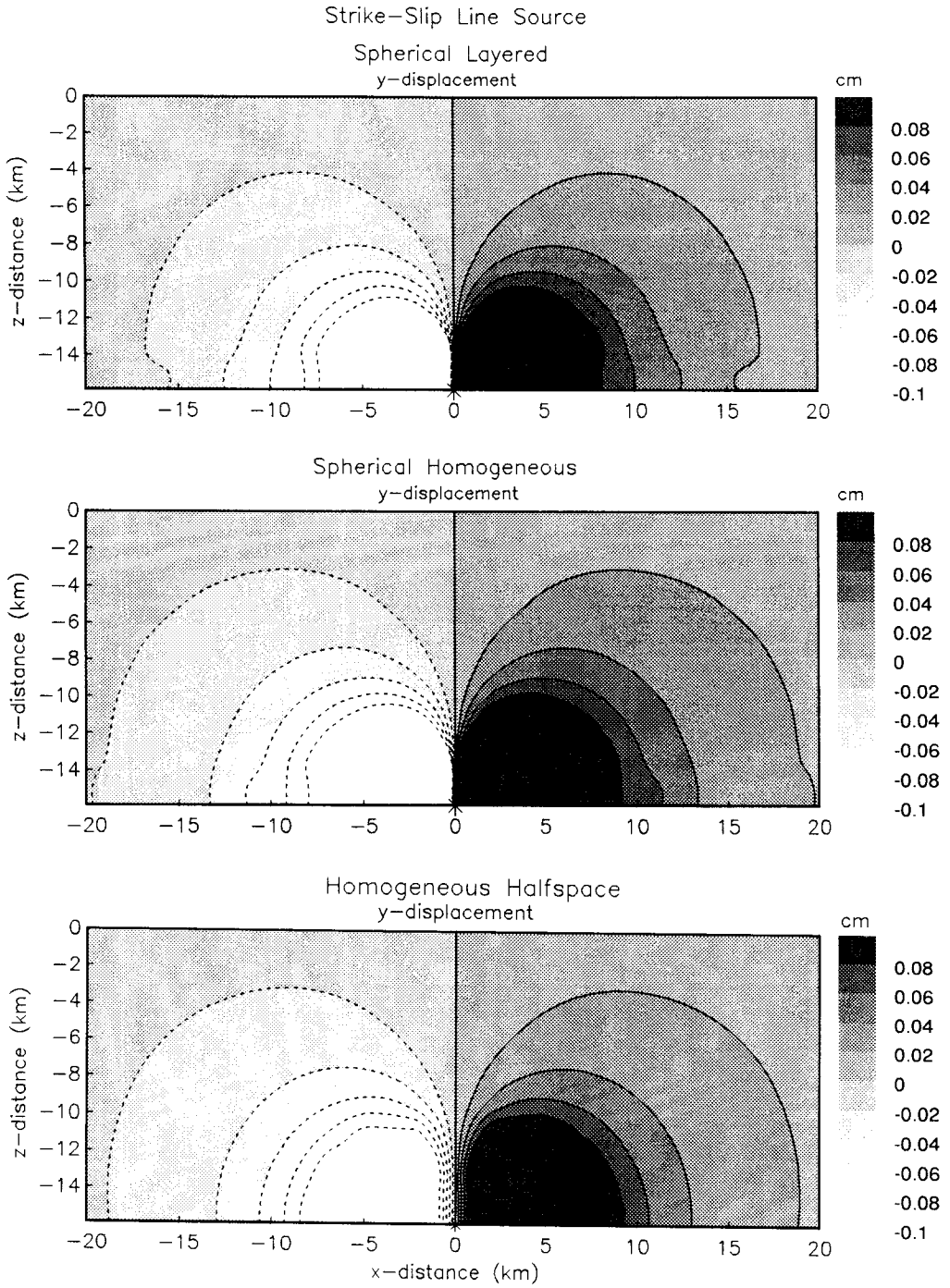

Figure 12. Depth profile of u_y for the strike-slip line source, taken in the plane defined by $y = 0$. The line source is placed at a depth of $d =$ 15.9 km (bottom of each panel). Displacement is unbounded as one approaches the source, but the contours are truncated for visual simplicity. The displacements in the layered case are clearly diminished relative to the homogeneous case. Slight distortion in the bottom 1 km of the spherical earth calculations is an effect of wavelength truncation at 1 km.

layered case. In particular, the top panel shows that the difference between the layered and homogeneous stresses is of opposite sign to the stresses themselves, showing that the stresses in the layered case are substantially diminished. Both the displacement and stress patterns are due to the increase in bulk and shear moduli at 16 km depth. It is expected that similar phenomena occur at all of the layer boundaries, particularly the Moho, with corresponding effects that depend on the source depth and the size of the jump in elastic parameters across these boundaries.

DEFORMATION AFTER COMPLETE RELAXATION

Many applications require the evaluation of crustal deformation in an elastic plate overlying a viscoelastic substrate (or

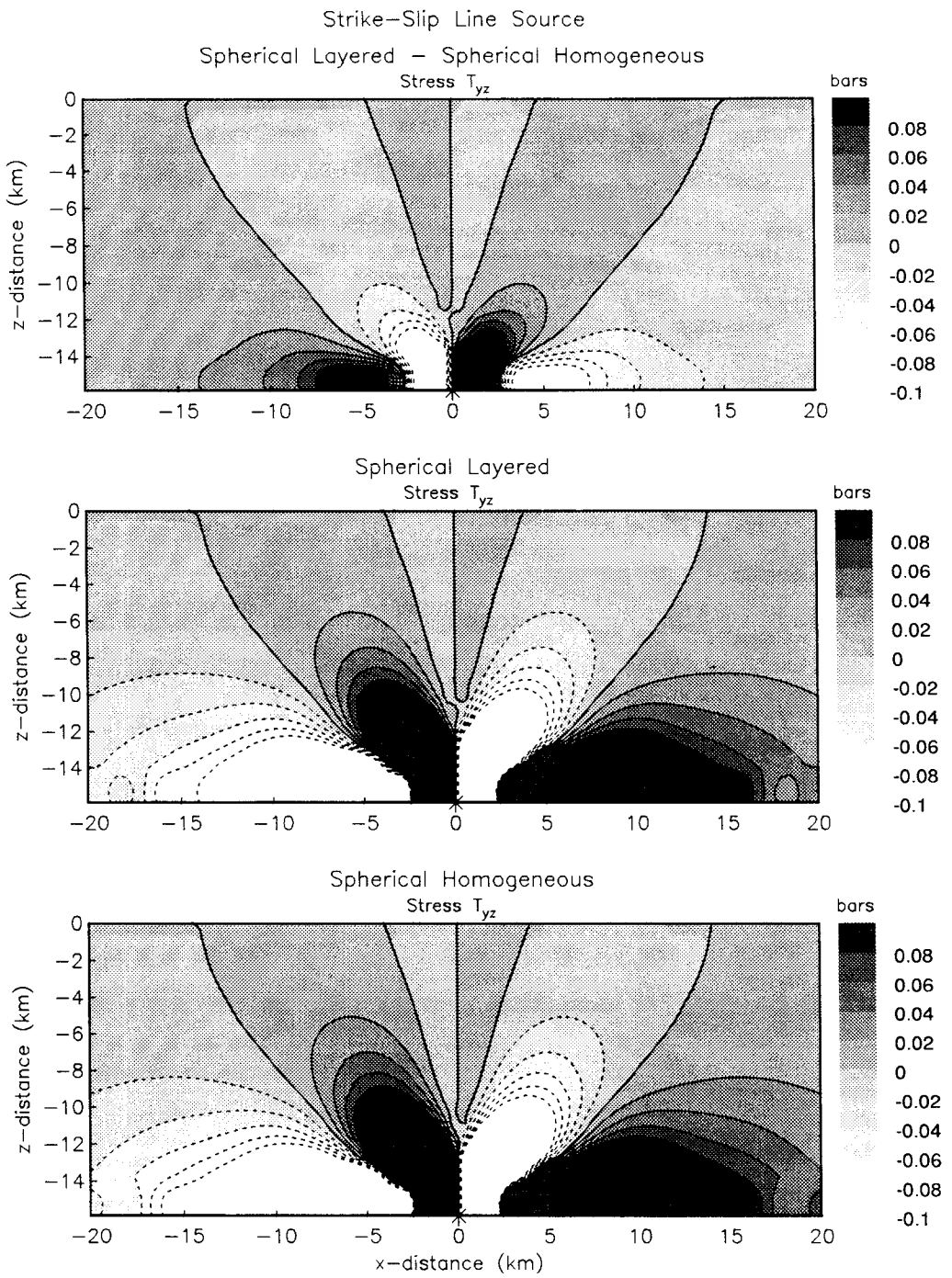

Figure 13. Depth profile of stress component T_{yz} for the strike-slip line source, taken in the plane defined by $y = 0$. The line source is placed at a depth of $d = 15.9$ km (bottom of each panel). The top panel shows the difference between the layered and homogeneous cases; its pattern is of opposite sign to the actual stress values, indicating smaller stresses in the layered case.

half-space) in the limit of complete relaxation following an earthquake (e.g. King, Stein & Rundle 1988). One method is to evaluate the post-seismic elastic deformation in the limit of complete relaxation and to add this to the initial coseismic deformation (Thatcher & Rundle 1979; King *et al.* 1988). As an alternative to this method, which generally depends on the accuracy of the inverse Laplace transforms, it is feasible to evaluate the deformation in the purely elastic layer directly by calculating the coseismic deformation subject to a fluid–solid boundary condition at a specified depth.

It is also straightforward to include gravitational restoring forces at this boundary, driven by the density contrast beween the elastic and ductile regions. Let $r = r_{\rm bot}$ define the top of a fluid region bounded above by solid material. Then, for spheroidal modes, the radial eigenfunctions are a linear combination of two independent solutions (Pollitz 1992),

$$\mathbf{y}^{(\rm I)}(r) = (l \quad 0 \quad 1 \quad 0)^{\rm T}, \tag{28a}$$

$$\mathbf{y}^{(\rm II)}(r) = (0 \quad 0 \quad 1 \quad 0)^{\rm T}. \tag{28b}$$

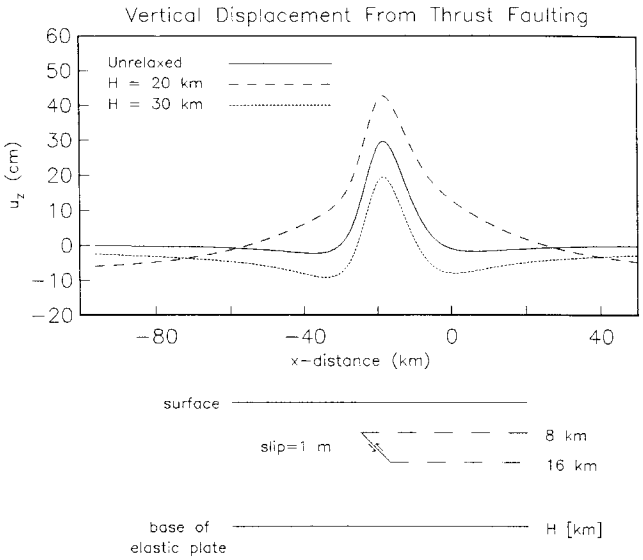

Figure 14. Comparisons among the displacements u_z for a finite thrust source, with different elastic plate thicknesses in the homogeneous sphere. The fault length is 50 km extending from $y = -25$ km to $y = 25$ km. The solid lines correspond to the coseismic deformation on the homogeneous sphere (without an elastic plate), and the dotted and dashed lines give the deformation for an elastic plate of thickness H bounded below by a fluid with gravitational restoring forces (eqs 28c and 29).

Solution (28a) does not include the effect of gravitational restoring forces at the interface $r = r_{bot}$. Such buoyancy effects may be accounted for by explicitly including the buoyancy force in the normal stress component $y_2^{(l)}$

$$\mathbf{y}^{(l)}(r) = [l \quad l(\Delta\rho)g_0 \quad 1 \quad 0]^T. \tag{28c}$$

In the above equation, g_0 is the acceleration due to gravity and $\Delta\rho$ is the difference between the asthenospheric density and the average lithospheric density. In the example to be shown here, I have assigned $\Delta\rho = 0.46\ \mathrm{g\,cm^{-3}}$. For toroidal modes, the boundary conditions are simply

$$\mathbf{y}^{(l)}(r) = (0 \quad 1)^T. \tag{29}$$

As an example, Fig. 14 shows a profile of vertical displacement u_z calculated from a finite thrust source, with different values of elastic plate thickness H. In these calculations, boundary conditions (28c) and (29) are applied at $r_{bot} = a - H$, and the minimum wavelength is 3.3 km. There is a strong sensitivity to elastic plate thickness, such that post-seismic (completely relaxed minus coseismic) uplift or depression is predicted, depending on which portion of the elastic plate is ruptured. For the case $H = 20$ km, much of the lower half of the elastic plate is ruptured, and post-seismic uplift is predicted. For the case $H = 30$ km, rupture is almost entirely in the upper part of the elastic plate, and post-seismic depression is predicted. These results are in excellent agreement with Fig. 7 of Cohen (1984), who calculated the elastic–gravitational post-seismic deformation for thrust faults which penetrate various portions of an elastic lithosphere overlying a viscoelastic asthenosphere.

CONCLUSIONS

A method for calculating the static deformation field on a layered spherical earth has been presented. This method is similar to that recently applied to the case of wave propagation on a layered spherical earth. It characterizes the seismic source in terms of jumps in the displacement–stress vector in order to determine the Green's functions directly. The deformation field is then obtained as a truncated sum of spheroidal and toroidal modes and can be readily calculated at both the Earth's surface and at depth. No numerical problems have been encountered in applying the method with cut-off wavelengths as small as 1 km. The method presented is also easily adapted to calculation of deformation in a layered elastic plate after complete relaxation of a ductile layer below the base of the elastic plate, which may include gravitational restoring forces at the base of the elastic plate.

Several comparisons among the spherical layered, spherical homogeneous, and homogeneous half-space cases have been presented. These demonstrate that the effect of sphericity is quite small out to at least 100 km from the epicentral region. The Earth's layering is characterized by sharp increases in the isotropic elastic parameters at the Conrad discontinuity and the Moho, assumed to be at depths 16 km and 33 km, respectively, in this paper. Relative to the spherical homogeneous earth, the effect of the Earth's layering is generally to diminish the calculated deformation for source depths shallower than 16 km and to enhance the deformation for source depths greater than 16 km. This result is analogous to the well-known seismic wave amplification/deamplification observed when seismic waves propagate across large impedence contrasts. Up to 20 per cent errors would be introduced in the calculated deformation fields for sources at crustal depths if the Earth's layering were not taken into account.

ACKNOWLEDGMENTS

Comments by two anonymous reviewers are appreciated. I thank Walter Zürn, Wolfgang Friederich and Ruedi Widmer for their helpful comments during the course of this work.

REFERENCES

Aki, K. & Richards, P.G., 1980. *Quantitative Seismology,* Vol. 1, W.H. Freeman & Co., San Fransisco, LA.

Ben-Menahem, A. & Singh, S.J., 1981. *Seismic Waves and Sources,* Springer–Verlag, New York, NY.

Cohen, S.C., 1984. Postseismic deformation due to subcrustal viscoelastic relaxation following dip-slip earthquakes, *J. geophys. Res.,* **89,** 4538–4544.

Dalkolmo, J., 1993. Synthetische Seismogramme fuer eine sphaerisch symmetrische, nichtrotierende Erde durch direkte Berechnung der Greenschen Funktion, *Diplomarbeit,* Institut für Geophysik, Universität Stuttgart.

Edmonds, A.R., 1960. *Angular momentum in quantum mechanics,* Princeton University Press, Princeton, NJ.

Friederich, W. & Dalkolmo, J., 1995. Complete synthetic seismograms for a spherically symmetric earth by a numerical computation of Green's function in the frequency domain, *Geophys. J. Int.,* **122,** 537–550.

Gilbert, F. & Dziewonski, A.M., 1975. An application of normal mode theory to the retrieval of structural parameters and source mechanisms from seismic spectra, *Phil. Trans. R. Soc. Lond.,* A., **278,** 187–269.

Jovanovich, D., Husseini, M.I. & Chinnery, M.A., 1974a. Elastic dislocations in a layered half-space—I. Basic theory and numerical methods, *Geophys. J. R. astr. Soc.,* **39,** 205–217.

Jovanovich, D., Husseini, M.I. & Chinnery, M.A., 1974b. Elastic

dislocations in a layered half-space—II. The point source, *Geophys. J. R. astr. Soc.*, **39,** 219–239.

King, G.C.P., Stein, R.S. & Rundle, J.B., 1988. The growth of geological structures by repeated earthquakes 1. Conceptual framework, *J. geophys. Res.*, **93,** 13 307–13 318.

Lapwood, E.R. & Usami, T., 1981. *Free Oscillations of the Earth,* Cambridge University Press, Cambridge.

Matsu'ura, M., Tanimoto, T. & Iwasaki, T., 1981. Quasi-static displacements due to faulting in a layered half-space with an intervenient viscoelastic layer, *J. Phys. Earth,* **29,** 23–54.

Okada, Y., 1985. Surface deformation due to shear and tensile faults in a half-space, *Bull. seism. Soc. Am.,* **75,** 1135–1154.

Okada, Y., 1992. Internal deformation due to shear and tensile faults in a half-space, *Bull. seism. Soc. Am.,* **82,** 1018–1040.

Pan, E., 1989. Static response of a transversely isotropic and layered half-space to general dislocation sources, *Phys. Earth planet. Inter.,* **58,** 103–117.

Pollitz, F.F., 1992. Postseismic relaxation theory on the spherical earth, *Bull. seis. Soc. Am.,* **82,** 422–453.

Rundle, J.B., 1980. Static elastic-gravitational deformation of a layered half-space by point couple sources, *J. geophys. Res.,* **85,** 5354–5363.

Rundle, J.B., 1982. Viscoelastic-gravitational deformation by a rectangular thrust fault in a layered Earth, *J. geophys. Res.,* **87,** 7787–7796.

Singh, S.J., 1970. Static deformation of a multilayered half-space by internal sources, *J. geophys. Res.,* **75,** 3257–3263.

Singh, S.J. & Garg, N.R., 1985. On two-dimensional dislocations in a multilayered half-space, *Phys. Earth planet. Inter.,* **40,** 135–145.

Takeuchi, H. & Saito, M., 1972. Seismic surface waves, in *Methods in Computational Physics: Seismology,* pp. 217–294, eds Bolt, B. Fernbach, S. and Rotenberg, M., Academic Press, New York, NY.

Thatcher, W. & Rundle, J.B., 1979. A model for the earthquake cycle in underthrust zones, *J. geophys. Res.,* **84,** 5540–5556.

Wason, H.R. & Singh, S.J., 1972. Static deformation of a multilayered sphere by internal sources, *Geophys. J. R. astr. Soc.,* **27,** 1–14.

Yoshioka, S., Hashimoto, M. & Hirahara, K., 1989. Displacement fields due to the 1946 Nankaido earthquake in a laterally inhomogeneous structure with the subducting Philippine Sea plate —a three-dimensional finite element approach, *Tectonophysics,* **159,** 121–136.